Image Fusion Processing for IKONOS 1-m Color Imagery

Kazi A. Kalpoma and Jun-ichi Kudoh, *Associate Member, IEEE*

Abstract—**Many image fusion techniques have been developed. However, most existing fusion processes produce color distortion in 1-m fused IKONOS images due to nonsymmetrical spectral responses of IKONOS imagery. Here, we proposed a fusion process to minimize this spectral distortion in IKONOS 1-m color images. The 1-m fused image is produced from a 4-m multispectral (MS) and 1-m panchromatic (PAN) image, maintaining the relations of spectral responses between PAN and each band of the MS images. To obtain this relation, four spectral weighting parameters are added with the pixel value of each band of the original MS image. Then, each pixel value is updated using a steepest descent method to reflect the maximum spectral response on the fused image. Comparison among the proposed technique and existing processes [intensity hue saturation (IHS) image fusion, Brovey transform, principal component analysis, fast IHS image fusion] has been done. Our proposed technique has succeeded to generate 1-m fused images where spectral distortion has been reduced significantly, although some block distortions appeared at the edge of the fused images. To remove this block distortion, we also proposed a sharpening process using a wavelet transform, which removed block distortion without significant change in the color of the entire image.**

Index Terms—**Histogram matching, IKONOS, image fusion process, spectral distortion, spectral response, steepest descent method, wavelet transform.**

I. INTRODUCTION

WITH high-resolution sensors, IKONOS (Advanced Earth Observing Satellite) provides both multispectral (MS) and panchromatic (PAN) data with spatial resolutions of 4 and 1 m, respectively. The MS images have four wavelength bands: red [R: 0.63–0.69 μm], green [G: 0.52–0.60 μm], blue [B: 0.45–0.52 μm], and near infrared [NIR: 0.76–0.90 μm]. The single-wavelength band for a PAN image is [0.45–0.90 μm]. Clearly visible being individual trees, automobiles, road networks, and houses, the IKONOS images allow for a more accurate understanding of phenomena on the ground [1]. High-resolution PAN images provide a better spatial quality compared with the MS images, and MS images provide a better spectral quality compared with the PAN images. To take advantage of the high space information of PAN images and the essential spectral information of MS images, image fusion is often an efficient and economical means to produce MS images with high spatial resolution, as well as essential spectral information. This image is important for a variety of remote sensing applications [2]. For example, in the geosciences domain, fused images can provide more detailed information for land use classification, change detection, map updating, and hazard monitoring; in national defense, it is useful for target detection, identification, and tracking, and in the medical imaging domain for diagnosis, modeling of the human body, or treatment planning.

Various image fusion processes have been proposed in the literature [1]–[17]. According to their efficiency in implementation, the intensity hue saturation (IHS) method [2]–[4], [14], principal component analysis (PCA) [5], [6], [17], and Brovey transform (BT) [6], [17] are the most commonly used algorithms in remote sensing applications. However, the problem of color distortion appears at the analyzed area after being transformed by using these fusion methods. The color distortion means the variation on hue after the fusion process, where hue is the property of the color determined by its wavelength [6].

Such a problem has been reported by many authors, such as Pellemans *et al.* [18] and Wang *et al.* [19], and have proposed a high-pass filtering (HPF) method. The main idea of HPF is to extract the spatial detail information from the PAN image, to later insert or inject it into the MS image previously expanded to match the PAN pixel size [11]. Several researchers have proposed a different method based on this, employing the discrete wavelet (DW) transform [20], [21], Laplacian pyramid algorithm [22], [23], or "á trous" wavelet transforms [24], [25] to perform the detail extraction and injection processes. Although the wavelet-based fusion (WBF) results provide better spectral quality than IHS [26], [27], the difference between the extracted spatial information and that existing in MS images can also introduce color distortion particularly when IKONOS, Quick-Bird, and Landsat-7 images are fused [2]. Moreover, WBF results depend on the number of decomposition levels, which is not a unique optimal number for images with a particular resolution ratio, rather than on the purpose of the fused images [28]. The filtering and subsampling process for DW decomposition could cause a loss of lineal continuity of spatial details [29]. Without subsampling, a DW decomposition scheme can only be applied to three-band RGB compositions [30].

In this paper, the IHS method, PCA, and BT have been compared. To find the cause of the variation on hue after the fusion process, a detailed study and analysis has been done, and two causes have been found. One is that the wavelength band of PAN of IKONOS extends into the area of NIR rays while the wavelength band of PAN for the other satellite is in

the area of the visible range. Influence of this NIR ray area of spectrum is ignored in existing fusion processes. Another cause is that the relationship of the spectral response between the PAN and each band of MS is not kept. Considering these two reasons, we proposed a fusion process to minimize the spectral distortion in IKONOS 1-m color images. To reflect the maximum spectral response on a fused image, four spectral weighting parameters are added to the pixel value of each band of original MS image. Steepest descent method [31] is used to update the pixel value of each band for each fused MS image. By this fusion process, the spectral response of each band of the original MS image was reflected in a 1-m MS fused image almost ideally, and the distortion of color information had been decreased significantly compared with the existing methods. However, a block distortion at the edge of the 1-m fused image appeared.

We investigated the causes and found that the block distortion corresponds to the high-frequency element of the image. Based on these, we also proposed a sharpening process using a wavelet transform only to remove this block distortion from the 1-m fused MS image, which was obtained by our proposed fusion process using the steepest descent method. The block distortion at the edge of the fused image has almost disappeared.

For this experiment, an IKONOS image of San Diego, CA, offered by Space Imaging Company is used. The size of the MS image is 125×125 pixels, and the size of the PAN image is 500×500 pixels. To verify our technique, the evaluation process has been done comparing to existing processes.

II. IMAGE FUSION PROCESS AND ITS PROBLEMS

The process of combining two or more images into a single image retaining important feature from each is called an image fusion process. When applying any IHS-based or wavelet-based image fusion methods, it is necessary that the high-resolution PAN image and low-resolution MS image be accurately superimposed. Therefore, as a preprocess, both images have to be coregistered, and the low-resolution MS image needs to be resampled to make their pixel size the same as that of the high-resolution PAN image [27]. The IKONOS image fusion process is a tool for integrating a high-resolution PAN 1-m image with an MS 4-m image, in which the resulting fused image contains both the high-resolution spatial information of the PAN image and the color information of the MS image.

A. IHS Image Fusion

IHS is one of the most widespread image fusion methods in remote sensing applications. The IHS transform is a technique where RGB space is replaced in the IHS space by intensity (I), hue (H), and saturation (S) level. The fusion process that uses this IHS transform is done by the following three steps.

1) First, it converts the RGB space into the IHS space (IHS transform).
2) The value of intensity I ($= (R + G + B)/3$) is replaced by the value of PAN.
3) The retransformed back into the original RGB space (reverse IHS transform).
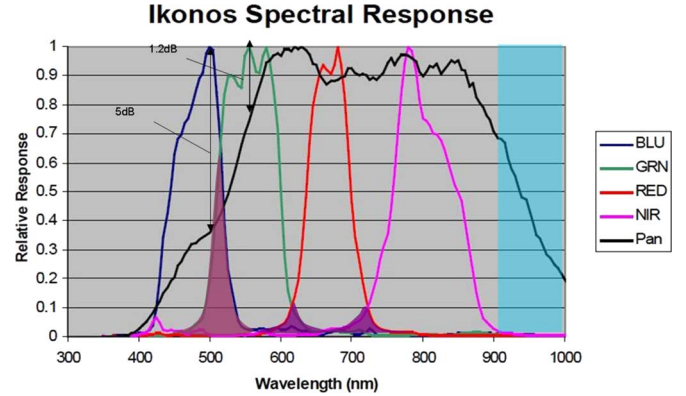

Fig. 1. Spectral response of the PAN and MS sensor of IKONOS.

B. PCA Method

The PCA technique is a decorrelation scheme used for various mapping and information extraction in remote sensing image data. The procedure to merge the RGB and the PAN image using the PCA fusion method is similar to that of the IHS method. The fusion process that uses this PCA is done by the following three steps.

1) First, it converts the RGB space into the first principal component (PC1), the second principal component (PC2), and the third principal component (PC3) by PCA.
2) The first principal component (PC1) of the PCA space is replaced by the value of the PAN image.
3) The retransformed back into the original RGB space (reverse PCA).

C. Brovey Transform (BT)

BT is a simple image fusion method that preserves the relative spectral contributions of each pixel but replaces its overall brightness with the high-resolution PAN image. The fusion process is done by applying the following conversion type to each pixel:

$$\begin{bmatrix} Rfi_i \\ Gfi_i \\ Bfi_i \end{bmatrix} = \frac{\text{PAN}}{I} \times \begin{bmatrix} R_i \\ G_i \\ B_i \end{bmatrix}. \qquad (1)$$

Here, R_i, G_i, and B_i are the pixel values of pixel i of each band, Rfi_i, Gfi_i, and Bfi_i are the pixel values of pixel i of each band that is obtained by fusion process, and $I = (R_i + G_i + B_i)/3$.

D. Problems on Existing Methods

When the existing image fusion processes like IHS, PCA, or BT are applied to the IKONOS images, spectral distortion appears, which means that the variation on hue before and after the fusion process has appeared. To find the cause of this variation on hue and to understand the influence of spectral response on the fused IKONOS images, the relative spectral responses, as shown in Fig. 1, are investigated in detail [32].

1) Frequency Band of IKONOS PAN Sensor: In a PAN sensor of SPOT or IRS, PAN imaging is performed in a

TABLE I
SPECTRAL RANGES OF DIFFERENT PAN IMAGES

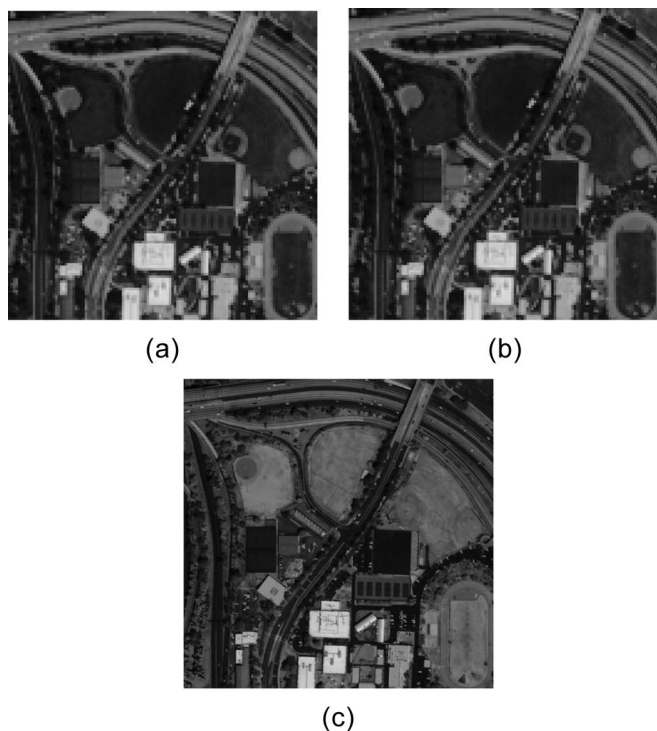| Satellite (name of sensor)	Frequency band
SPOT (HRV, HRG)	0.51~0.73μm
IRS (PAN)	0.50~0.75μm
IKONOS (PAN)	0.45~0.90μm

Fig. 2. Comparison among the brightness (light and shade) of intensity, PC1, and PAN images. The scene is an IKONOS image of San Diego, CA. (a) Intensity image. (b) First principle component: PC1 image. (c) PAN image.

single spectral band, corresponding to the visible part of the electromagnetic spectrum. The PAN band covers 0.51–0.73 μm and is a narrow bandwidth. But the PAN sensor of IKONOS performs the PAN imaging in a single spectral band (0.45–0.90 μm) corresponding from the visible to NIR area.

Table I shows the wavelength (frequency band) of several PAN images. On early method like IHS conversion, required intensity $I (= (R + G + B)/3)$ is calculated by averaging the pixel values of R, G, and B in each pixel, i.e., the influence of the NIR ray area of spectrum is ignored closely. Also, intensity I is replaced by the value of the PAN image. When we compared the light and shade (brightness) of the intensity image and the PAN image for a particular scene, it is found that the step value of each pixel differs.

As an example, the intensity image and the PAN image are shown in Fig. 2(a) and (c). Since the PAN image and the intensity image are different, a spectral distortion is caused in the IHS conversion, and the hue (color tone) changes before and after the fusion process. This also influenced the changes on hue for the BT as the calculation value of PAN/I in (1) becomes a value away from 1. Same as IHS conversion, in PCA conversion, PC1 image is replaced with PAN image, and their values of light and shade differ which influence the change on

hue after the fusion process. To reduce the color distortion, it is essential to include the response of NIR band into I.

2) Spectral Response of IKONOS PAN and MS Sensors: Fig. 1 shows that the level of the spectral response of each band of MS (R, G, B, and NIR, respectively) and the spectral response of PAN is different in an arbitrary frequency. At the frequency of the peak level of B-band (about 500 nm), the spectral response of B is larger than PAN level, and the difference is about $10 \log_{10} (1/0.35) \simeq 5$ dB. The level of G-band (at about 560 nm) is about 1.2 dB larger than the level of the PAN band, and band R is also a little high. B- and G-bands overlapped substantially (marked as pink area in Fig. 1). Furthermore, the PAN wavelength band extended beyond the NIR band but the spectral response of NIR (about 900–1000 nm) does not exist on PAN response. Obviously, color distortion problem in the fusion process resulted from these mismatches.

Tu *et al.* [6] also demonstrated that the hue component in the IHS space is unchanged, and the altered saturation component results in the color distortion. A study of the color distortion problem arising from the spectral mismatch between PAN and MS bands is presented, and a simple spectral-adjusted scheme by using two weights is proposed with the integration of a fast IHS fusion method [1]. This approach provides a better spectral response than the original IHS but sacrifices the spatial information. Using this fast IHS, Choi [33] proposed a new IHS approach image fusion with a tradeoff parameter to control the tradeoff between the spatial and the spectral resolution of the image to be fused.

In 2005, Zhang and Hong [2] utilize the IHS transform to fuse the high-resolution spatial information into low-resolution MS image and use the wavelet transform to reduce the color distortion, in a way of generating a new high-resolution PAN image that correlates to the intensity image of the IHS transform. The new PAN image is, then, used to replace the intensity image for a reverse IHS transform. The fused image is produced after the reverse IHS transform. The fusion results were better than the conventional IHS methods. Since the PAN and the intensity are not spectrally similar and the effect of the NIR bands is not included in I (intensity image), from such mismatches, results of color distortion problem happen in this scheme.

To include the response of the NIR band and to solve the problem of spectral mismatches, as discussed above, four spectral weighting parameters are added with the pixel value of each band of MS image, and the steepest descent method [31] is used to update the pixel value of each band of fused MS image repeatedly until the color distortion becomes minimum.

III. PROPOSED METHOD

In the preceding paragraphs, the problems on early methods are enumerated. For IKONOS images, it is thought that the relation of the pixel value of PAN and each band of MS (R, G, B, and NIR) will be maintained by putting four parameters.

In our fusion technique, four parameters (w_R, w_G, w_B, and w_{NIR}) are added as weight with the pixel value of each band of MS (R, G, B, and NIR) image, and the following relation (2) is assumed [34], [35]. Then, in the fusion process, each pixel value of R, G, B, and NIR is corrected in a way that (2) may

consist of the response between each band of MS (R, G, B, and NIR) and PAN in

$$\text{PAN} \cong w_R \times R + w_G \times G + w_B \times B + w_{\text{NIR}} \times \text{NIR} \qquad (2)$$

fused image. To do so, first, energy function E is defined later in other paragraph, and steepest descent method [31] is used to minimize the function E.

A. Steepest Descent Method

The steepest descent method is one of the search method used in the minimization (or maximization) problem of PAN-function $f(\mathbf{u})$ of variable $\mathbf{u} = (u_1, u_2, u_3, \ldots, u_n)^{\text{T}}$. It approaches the minimum in a manner where it goes into the direction in which $f(\mathbf{u})$ decreases most quickly. The search starts at an initial point $\mathbf{u}^{(0)}$, and to search for the route to the lowest (or highest) point u^* in the terminal, it pays attention to the preference close enough to the solution of $f(\mathbf{u})$.

It is a problem of reaching the deepest part from the edge of the print plectrum when assuming the minimization problem of $f(\mathbf{u})$. It is assumed that it leaves $\mathbf{u}^{(0)}$ around the print plectrum, it advances horizontally with constant step Δ, and it goes down to point $\mathbf{u}^{(k)}$ of times k. This procedure knows the following descent point of slope in advance. The method simply takes a step Δ in the direction where the mountain gets off. In other words, the iterative procedure, to make Δ changes of ith component to the direction where the slope is decreased, is as follows:

$$u_i^{(k+1)} = u_i^{(k)} - \Delta \frac{\partial f(u^{(k)})}{\partial u_i^{(k)}}. \qquad (3)$$

Vector $(\partial f(u)/\partial u_1, \partial f(u)/\partial u_2, \ldots, \partial f(u)/\partial u_n)$ has a downward direction with a maximum change rate of $f(u)$; a vertical direction to the contour line of PAN-function $f(u)$ is indicated.

B. Definition of Energy Function

Energy function E is defined in terms of the square error margin with the corresponding weight of the pixel value of each pixel of each band of MS (R, G, B, and NIR) and the corresponding pixel value of PAN image as shown in (4). The pixel value is updated repeatedly until this E is minimized.

$$E = \sum_{i=0}^{M-1} \sum_{j=0}^{N-1} \Big(\big(w_R \times Rfi(i,j) + w_G \times Gfi(i,j) + w_B \\ \times Bfi(i,j) + w_{\text{NIR}} \times \text{NIR}fi(i,j)\big) \\ - \text{PAN}(i,j) \Big)^2. \qquad (4)$$

Here, $Rfi(i,j)$, $Gfi(i,j)$, $Bfi(i,j)$, and $\text{NIR}fi(i,j)$ ($0 \leq i \leq M-1$, $0 \leq j \leq N-1$) are the pixel values of each band at the coordinate (i,j) of fused MS image. w_R, w_G, w_B, and w_{NIR} are constant.

If we assume that E is a function of the variables $Rfi(i,j)$, $Gfi(i,j)$, $Bfi(i,j)$, and $\text{NIR}fi(i,j)$, then by minimizing the
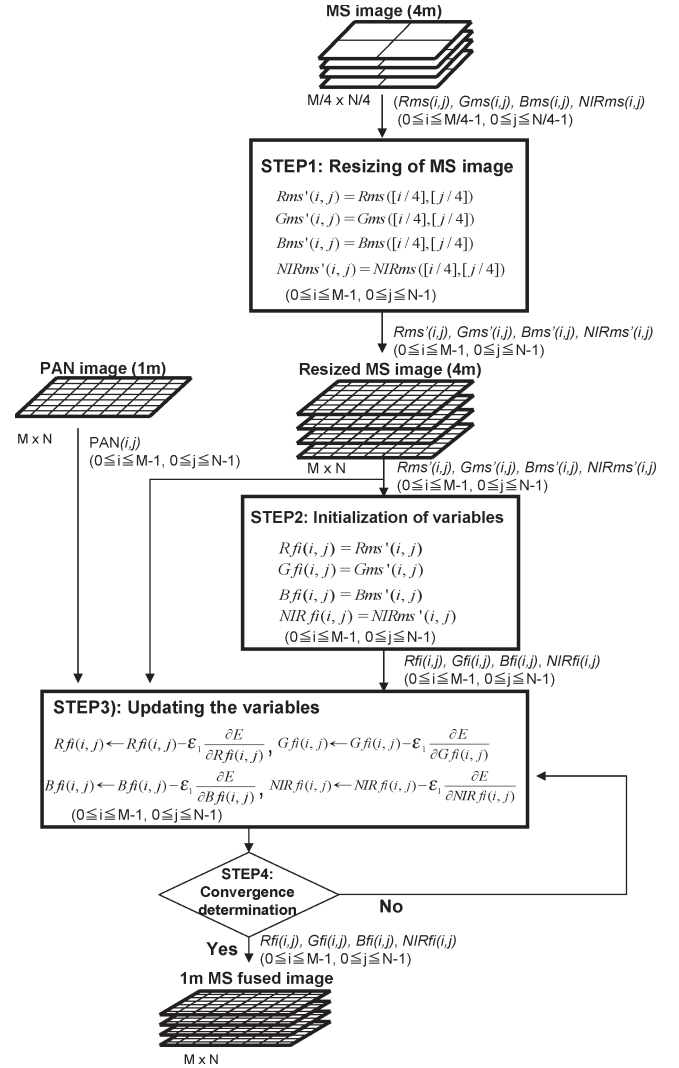

Fig. 3.   Schematic flowchart of the proposed algorithm.

energy function E of (4), the pixel value of the fused image that fills (2) can be achieved.

C. Proposed Algorithm

The proposed technique is composed of four steps, as shown in Fig. 3. The MS image is expanded to the same size as the PAN image, in order to get perfectly superposable images [27]. As a preprocessing (STEP1), the pixel value of the fused MS images is initialized (STEP2), and to minimize the energy function, the steepest descent method is used, and the pixel value is updated repeatedly (STEP3). Also, the convergence determination is processed to end the update process (STEP4). The methodology of each step is explained in following paragraph.

1) STEP1—Resizing of MS Image: The MS image is resized, i.e., the size of the MS image is expanded to the same size as the PAN image, in order to get perfectly superposable images [27]. To process it, nearest neighbor methodology is used here. The pixel of the MS image at the same position as the pixel of the PAN image is made correspondence (Fig. 4). Since IKONOS PAN and MS images are 1- and 4-m resolutions,
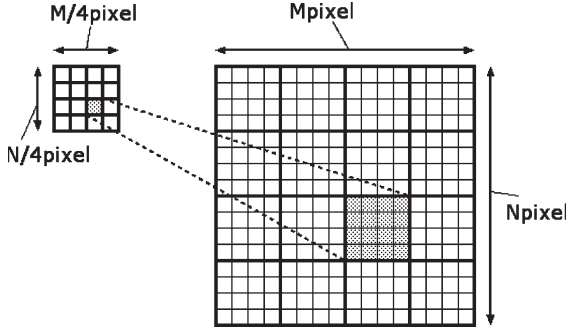
Fig. 4. Resizing of MS image (Left: Original MS image, Right: Resized MS image).

respectively, when the PAN image size is assumed to be $M \times N$, the image size of the MS image becomes $M/4 \times N/4$.

To change the size of the MS image into $M \times N$, the pixel values ($R\mathrm{ms}(i,j)$, $G\mathrm{ms}(i,j)$, $B\mathrm{ms}(i,j)$, $\mathrm{NIR}\mathrm{ms}(i,j)$) ($\backslash 0 \leqq i \leqq M/4 - 1$, $0 \leqq j \leqq N/4 - 1$) of each band of images (R, G, B, and NIR) are applied in the following

$$R\mathrm{ms}'(i,j) = R\mathrm{ms}\left([i/4],[j/4]\right) \tag{5}$$

$$G\mathrm{ms}'(i,j) = G\mathrm{ms}\left([i/4],[j/4]\right) \tag{6}$$

$$B\mathrm{ms}'(i,j) = B\mathrm{ms}\left([i/4],[j/4]\right) \tag{7}$$

$$\mathrm{NIR}\mathrm{ms}'(i,j) = \mathrm{NIR}\mathrm{ms}\left([i/4],[j/4]\right). \tag{8}$$

$R\mathrm{ms}'(i,j)$, $G\mathrm{ms}'(i,j)$, $B\mathrm{ms}'(i,j)$, and $\mathrm{NIR}\mathrm{ms}'(i,j)$ ($0 \leqq i \leqq M - 1$, $0 \leqq j \leqq N - 1$) from (5)–(8) are the pixel values of the resized MS images of (R, G, B, and NIR).

When the MS image was expanded to $M \times N$ with this nearest neighbor method, it did not introduce any new data into the resized MS image. In fact, the data were preserved as in the original image exactly; every source point is used in the extended image.

2) STEP2—Initialization of Variables: In the fusion process, variables of energy functions for each pixel value of the fused MS image are initialized. Each pixel value of the fused MS image, $Rfi(i,j)$, $Gfi(i,j)$, $Bfi(i,j)$, and $\mathrm{NIR}fi(i,j)$ variables of energy function E are set to each pixel value of expanded MS images to which ($0 \leqq i \leqq M - 1$, $0 \leqq j \leqq N - 1$) in the following

$$Rfi(i,j) = R\mathrm{ms}'(i,j) \tag{9}$$

$$Gfi(i,j) = G\mathrm{ms}'(i,j) \tag{10}$$

$$Bfi(i,j) = B\mathrm{ms}'(i,j) \tag{11}$$

$$\mathrm{NIR}fi(i,j) = \mathrm{NIR}\mathrm{ms}'(i,j). \tag{12}$$

Pixel values of variables initialized by (9)–(12) are repeatedly updated until the energy function E is minimized by using the update rule described in the next paragraph.

3) STEP3—Updating the Variables: Updating of the variables of energy functions for each pixel value of each band is repeated based on the initial value decided in the foregoing paragraph (STEP2). The update of the pixel value is shown

by (13)–(16), where ε_1 is constant and a very small positive number.

$$Rfi(i,j) \leftarrow Rfi(i,j) - \varepsilon_1 \frac{\partial E}{\partial Rfi(i,j)} \tag{13}$$

$$Gfi(i,j) \leftarrow Gf(i,j) - \varepsilon_1 \frac{\partial E}{\partial Gfi(i,j)} \tag{14}$$

$$Bfi(i,j) \leftarrow Bfi(i,j) - \varepsilon_1 \frac{\partial E}{\partial Bfi(i,j)} \tag{15}$$

$$\mathrm{NIR}fi(i,j) \leftarrow \mathrm{NIR}fi(i,j) - \varepsilon_1 \frac{\partial E}{\partial \mathrm{NIR}fi(i,j)}. \tag{16}$$

4) STEP4—Convergence Determination: After the pixel value is updated in the foregoing paragraph (STEP3), the convergence determination is done by (17)–(20). When (17)–(20) are all true, the process is completed. Otherwise, STEP3's process is executed again. Here, ε_2 is constant and a very small positive number.

$$\sum_{i=0}^{M-1} \sum_{j=0}^{N-1} \frac{\partial E}{\partial Rfi(i,j)} < \varepsilon_2 \tag{17}$$

$$\sum_{i=0}^{M-1} \sum_{j=0}^{N-1} \frac{\partial E}{\partial Gfi(i,j)} < \varepsilon_2 \tag{18}$$

$$\sum_{i=0}^{M-1} \sum_{j=0}^{N-1} \frac{\partial E}{\partial Bfi(i,j)} < \varepsilon_2 \tag{19}$$

$$\sum_{i=0}^{M-1} \sum_{j=0}^{N-1} \frac{\partial E}{\partial \mathrm{NIR}fi(i,j)} < \varepsilon_2. \tag{20}$$

When the process is completed, $Rfi(i,j)$, $Gfi(i,j)$, $Bfi(i,j)$, and $\mathrm{NIR}fi(i,j)$ ($0 \leqq i \leqq M - 1, 0 \leqq j \leqq N - 1$) are pixel values of 1-m MS images. It means that, when ($0 \leqq i \leqq M - 1, 0 \leqq j \leqq N - 1$)

$Rfi(i,j)$ pixel values of 1-m R image;
$Gfi(i,j)$ pixel values of 1-m G image;
$Bfi(i,j)$ pixel values of 1-m B image;
$\mathrm{NIR}fi(i,j)$ pixel values of 1-m NIR image.

D. Decision of Values ε_1 and ε_2

ε_1 and ε_2 are used in (13)–(16) and (17)–(20), respectively. It is necessary to set an appropriate value to ε_1 and ε_2 in the fusion process. The values of ε_1 and ε_2 are decided as follows.

1) Value of ε_1: If a large value of ε_1 is given during the updating of the pixel value in STEP3, there is a possibility of taking the pixel value which is a negative value or larger than 255 (when 8 pixel/b). On the other hand, if a small value of ε_1 is given, the frequency of update which is done in STEP3 increases, and the processing time becomes long. Therefore, it is necessary to give a suitable value for ε_1. Changing the value of ε_1, it has been examined how the mean value of the pixel values of each band changed at each update.

Fig. 5 shows an example when $w_R = 0.25$, $w_G = 0.25$, $w_B = 0.25$, and $w_{\mathrm{NIR}} = 0.25$ are taken. In Fig. 5, when the value of ε_1 is given as 0.01, 0.1, and 1, comparatively, the change was almost the same. Also, when ε_1 is assumed to be
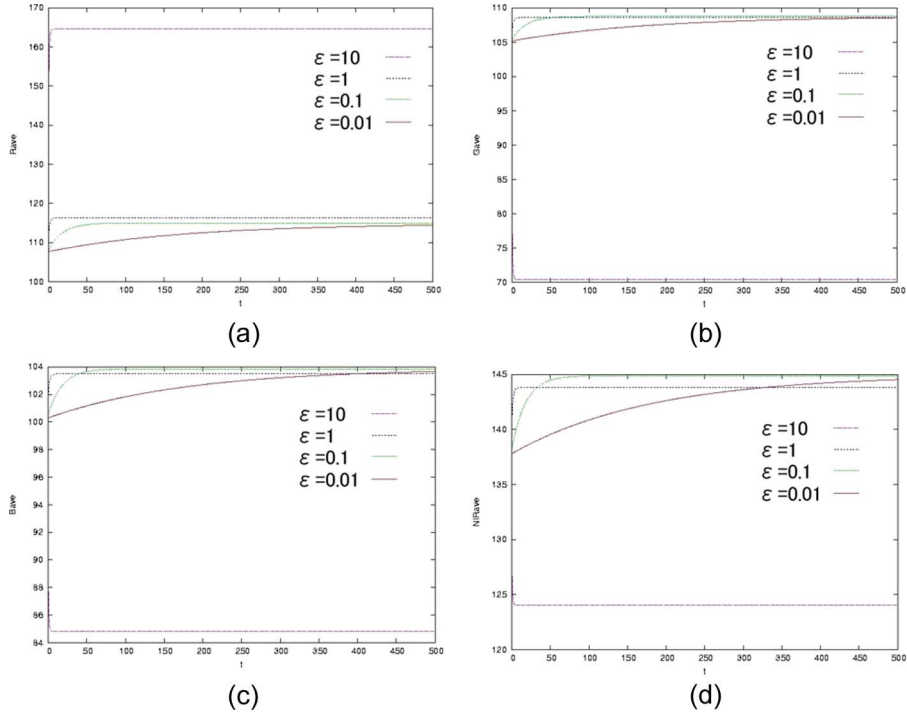
Fig. 5.   Relation of average of gray value for each band on update times t ($w_R = 0.25, w_G = 0.25, w_B = 0.25, w_{\mathrm{NIR}} = 0.25$). (a) R band. (b) G band. (c) B band. (d) NIR band.

ten, the change in the value differs from the time of 0.01, 0.1, and 1. It is not suitable. From the analysis, it is understood that, if ε_1 is given a value smaller than one, the change in the value will be the same as when ε_1 is given a very small value. In this paper, the value of ε_1 is set to 0.5.

2) Value of ε_2: If ε_1 is not set to a small enough value in the convergence-determination process, there is a possibility that processing will end without getting enough settlement for the energy function. Here, "enough settlement" means "it settles to the state that all pixel values do not change." During the convergence determination, the values of the partial differential of (17)–(20) for each pixel are assumed to be the variables with values smaller than the average of $\varepsilon_2/(N \times M)$. The pixel value will be changed by only one update on average $(0.5 \times \varepsilon_2)/(N \times M)$ as follows, because each partial differential in (17)–(20) is multiplied by $\varepsilon_1 = 0.5$ which is set in the foregoing paragraph. If it is adjusted to $\varepsilon_2 = 10\,000$, as the sizes of the image used by the evaluation are 500×500, $(0.5 \times 10\,000)/(500 \times 500) = 0.02$ or less, and the change in the pixel value can make it settle enough. Here, it made $\varepsilon_2 = 10\,000$.

IV. EXPERIMENTAL RESULTS AND EVALUATION

To illustrate our fusion process with an example, the data used for this experiment are IKONOS image of San Diego, CA, offered by Space Imaging Company. The size of the MS image is 125×125 pixels at a resolution of 4 m, and the size of the PAN image is 500×500 pixels at a resolution of 1 m [Fig. 6(a)–(c)].

Our fusion process is tested and shown in Fig. 6(d). To verify the efficiency of our proposed technique, two kinds of

(a) MS image (band: R G B, resolution: 4m)   (b) MS image (band: NIR, resolution: 4m)

(c) Original PAN image (band: PAN, resolution: 1m)   (d) Fused MS image (w_R=0.2, w_G=0.2, w_B=0.1, w_{NIR}=0.3, band: R G B, resolution: 1m)
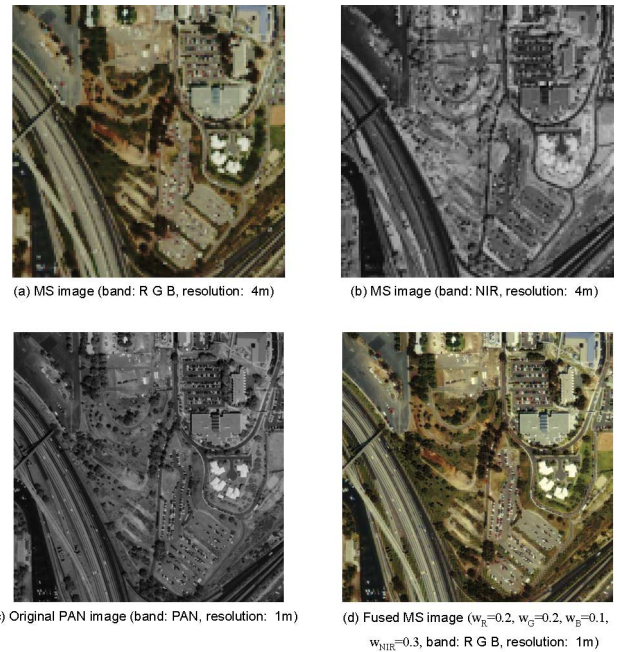
Fig. 6.   Scene is an IKONOS image of San Diego, CA. (a), (b), and (c) Original images offered by Space Imaging Company. (d) Fused 1-m color image that is produced by the proposed technique. The sizes of (a) and (b) are 125×125 pixels, and the size of (c) is 500×500 pixels.

evaluation have been done: evaluation by value of parameters and comparison with the existing techniques, as described in the next paragraphs. The spectral quality of the fused images is evaluated by comparing their spectral information to that of the original IKONOS low-resolution images. This comparison is

TABLE II
"CORRELATION COEFFICIENT BETWEEN MS IMAGE AND FUSED MS IMAGE" AND "CORRELATION COEFFICIENT BETWEEN PAN IMAGE AND THE INTENSITY IMAGE OF FUSED MS IMAGE" BY w_R, w_G, w_B, w_{NIR}, AND ave = $(r_R + r_G + r_B)/3$

w_R	w_G	w_B	w_{NIR}	rR	rG	rB	ave	rPAN	rH
0.0	0.4	0.1	0.3	1.000	0.806	0.986	0.931	0.876	0.233
0.0	0.5	0.1	0.3	1.000	0.781	0.994	0.925	0.877	0.252
0.1	0.3	0.1	0.3	0.976	0.822	0.974	0.924	0.893	0.478
0.1	0.4	0.0	0.3	0.986	0.809	1.000	0.932	0.883	0.469
0.1	0.5	0.0	0.3	0.991	0.775	1.000	0.922	0.887	0.486
0.2	0.2	0.1	0.3	0.894	0.898	0.967	0.920	0.885	0.650
0.2	0.3	0.0	0.3	0.925	0.854	1.000	0.926	0.886	0.449

performed both visually and quantitatively using the following indicators.

1) Correlation coefficient between the original and the fused images. It should be as close to 1 as possible.
2) The *erreur relative globale adimensionnelle de synthèse* (ERGAS) index or relative dimensionless global error in synthesis in fusion [25] as follows:

$$\text{ERGAS} = 100\frac{h}{l}\sqrt{\frac{1}{N_{\text{Bands}}}\sum_{i=1}^{N_{\text{Bands}}}\left(\frac{\text{rmse}^2(\text{Band}_i)}{\text{MS}_i}\right)} \quad (21)$$

h spatial resolution of PAN;
l spatial resolution of MS;
N_{Bands} number of bands of the fused images;
MS_i mean radiance value of the ith band of MS

and

$$\text{rmse}(\text{Band}_i) = \frac{1}{\text{NP}}\sqrt{\sum_{k=1}^{\text{NP}}(\text{MS}_i(k) - \text{FUS}_i(k))^2}. \quad (22)$$

Here
  NP   number of pixels of the fused images;
  FUS_i radiance value of the ith band of the fused images;
  MS_i radiance value of the ith band of the MS images.
The lower the value of the ERGAS index, the higher the spectral quality of the fused image.

The correlation coefficient between the original MS (R, G, and B) image and the fused image, and their average value have been compared for the correctness of the spectral quality. Also, for the spatial quality evaluation, the correlation coefficients between the PAN image and the intensity image of the fused MS images have been compared. Moreover, the comparison among the proposed technique and the existing processes (IHS, BT, PCA, and fast IHS by two weighting parameter) has been done.

A. Evaluation by Value of Parameters

The values of the four spectral weighting parameters w_R, w_G, w_B, and w_{NIR} cannot be theoretically modeled and determined; their selection is related to fusion results, by observing directly the image result. When the parameters w_R, w_G, w_B, and w_{NIR} are set to some respective values, it is analyzed whether or not it obtains the image that reflected spatial resolution of PAN and spectrum information of the MS images, respectively. First of all, each value of w_R, w_G, w_B, and w_{NIR} is set to 0.0, 0.1, 0.2, ..., 1.0 of 11 kinds, and in total, 11^4 fused MS images were generated in the fusion processes. Three kinds of correlation coefficients are calculated by changing and comparing the values of the parameters w_R, w_G, w_B, and w_{NIR}. Partial results have been listed in Table II and Fig. 7.

The correlation coefficient (rR, rG, and rB) between the original 4-m MS image (R, G, and B) and the fused 1-m MS image, the correlation coefficient (rPAN) between the PAN image and the intensity image of the fused image, and the correlation coefficient (rH) between the 4-m MS color (hue) and the 1-m fused image (hue) have been calculated and compared.

First of all, the image in which the resolutions of the PAN image and the spectrum information of the MS images are reflected well is chosen. Then, the correlation coefficients rR, rG, rB, and rPAN are used. It can be said that rR, rG, and rB will maintain the spectrum information of the former MS images by taking a value close to one. Moreover, it can be said that the resolution of the PAN image will be reflected by taking a value of rPAN close to one.

When changing the parameter values, the relation of the tradeoff in the values of rR, rG, rB, and rPAN has to be understandable. When the parameters are set so that the values of rR, rG, and rB may reach a value close to one as much as possible, the value of rPAN takes a value far from one. Oppositely, when the parameters are set so that the value of rPAN may reach a value close to one as much as possible, the values of rR, rG, and rB takes a value far from one.

When the values of rPAN, rR, rG, and rB reach far from one, the resolution of the former PAN image cannot be reflected. The resolution of the former MS image becomes a bad image, and the spectrum information of the former MS image will be lost.
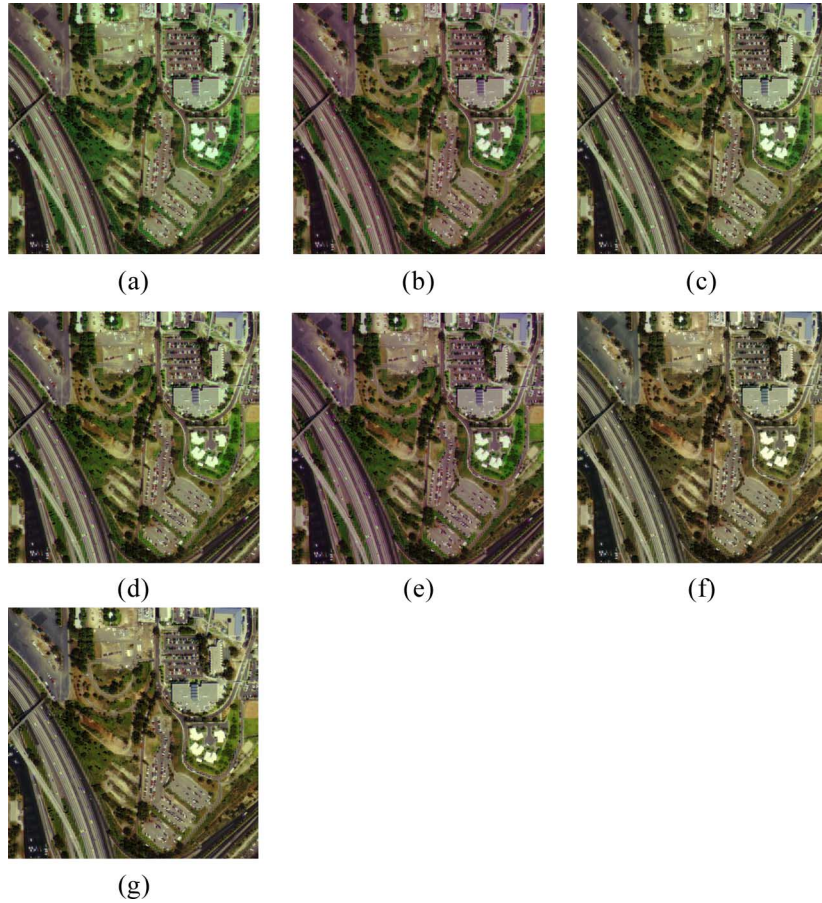
Fig. 7. One-meter MS fused image (R, G, and B) with different values of parameters w_R, w_G, w_B, and w_{NIR}. (a) $w_R = 0$, $w_G = 0.4$, $w_B = 0.1$, and $w_{NIR} = 0.3$. (b) $w_R = 0$, $w_G = 0.5$, $w_B = 0.1$, and $w_{NIR} = 0.3$. (c) $w_R = 0.1$, $w_G = 0.3$, $w_B = 0.1$, and $w_{NIR} = 0.3$. (d) $w_R = 0.1$, $w_G = 0.4$, $w_B = 0$, and $w_{NIR} = 0.3$. (e) $w_R = 0.1$, $w_G = 0.5$, $w_B = 0$, and $w_{NIR} = 0.3$. (f) $w_R = 0.2$, $w_G = 0.2$, $w_B = 0.1$, and $w_{NIR} = 0.3$. (g) $w_R = 0.1$, $w_G = 0.3$, $w_B = 0.1$, and $w_{NIR} = 0.3$.

From this point, it is very necessary to set the parameter in such a way that the values of rR, rG, rB, and rPAN all take a high value.

The fused MS images (bands: R, G, and B) generated for each set of parameter in Table II are shown in Fig. 7(a)–(g).

When seven images of Fig. 7(a)–(g) are compared with the original MS images, the changes in hue are understood. For example, in Fig. 7(a), the color in overall vegetation areas is green and becomes so vivid. From this, it is understood that the standard is not evaluated only by the values of rR, rG, rB, and rPAN but also by how much the hue of the former image is preserved and shown. In this respect, we included the correlation coefficient (rH) between the 4-m MS color (hue) and the 1-m fused image (hue) in Table II, and compared. However, hue H is calculated by using the conversion of HS16 pyramid color model. Then, rH takes the highest value at $w_R = 0.2$, $w_G = 0.2$, $w_B = 0.1$, and $w_{NIR} = 0.3$. It can be said that the image at $w_R = 0.2$, $w_G = 0.2$, $w_B = 0.1$, and $w_{NIR} = 0.3$ [Fig. 6(d), Fig. 7(f)] in which the hue of the original MS image is reflected most.

According to the experimental results, the best weighting parameters of w_R, w_G, w_B, and w_{NIR} of R, G, B, and NIR bands are chosen as 0.2, 0.2, 0.1, and 0.3, respectively, where the mean value of rR, rG, and rB is 0.920 and the value of

rPAN is 0.885 (Table II). Using these values, next, the comparison among the proposed technique and the existing processes is done.

B. Comparison With the Existing Techniques

Comparison among the proposed technique and the existing four fusion processes (IHS, BT, PCA, and fast IHS fusion) is done. The correlation coefficient is calculated globally for the entire image, and to estimate the global spectral quality of the fused images, the ERGAS index [25] is used. The results are shown in Table III. The overall results indicated that the correlation coefficient factors coincide with the ERGAS index values.

Table III contains the fusion results of the IHS method, BT method, PCA method, and fast IHS method proposed by Tu *et al.* [1] and the proposed method. The results show that the spectral quality of the fused images obtained by the proposed method is improved.

Our average correlation coefficient value of rR, rG, and rB (ave in Table III) is 0.920, which is increased by more than 0.3 when compared with the other three conventional processes, IHS, BT, and PCA. Also, the value of the ERGAS index for the proposed method decreased significantly. Moreover,

TABLE III
COMPARISON OF THE PROPOSED TECHNIQUE WITH THE EXISTING TECHNIQUES: $w_R = 0.2$, $w_G = 0.2$, $w_B = 0.1$, $w_{\text{NIR}} = 0.3$, AND ave $= (r_R + r_G + r_B)/3$

		r_R	r_G	r_B	Ave	r_{PAN}	ERGAS index
IHS		0.604	0.571	0.565	0.580	0.998	2.722
BT		0.609	0.538	0.590	0.579	0.997	2.653
PCA		0.627	0.538	0.585	0.583	0.995	4.089
Fast IHS [1]		0.856	0.893	0.996	0.915	0.867	1.603
Proposed method	Before wavelet	0.894	0.898	0.967	0.920	0.885	1.384
	After wavelet	0.859	0.865	0.907	0.877	0.898	1.727

comparing with fast IHS fusion process [1] that allows obtaining high-resolution images with better spectral quality [27], the correlation values for our method in both cases (ave and rPAN) are increased, and the ERGAS index value (1.384) has decreased (from 1.603). Higher correlation coefficient or lower ERGAS values of the proposed method than the existing methods (in Table III) indicate that the analyzed image fusion procedure that uses steepest descent method allows a high-quality transformation of the MS content while the spatial resolution is increased. Therefore, our proposed method significantly reduced the spectral distortion compared with the other existing processes.

Correlation coefficient value of rPAN for our proposed method is 0.885, which decreased slightly (0.1) compared with the three conventional methods. However, it increased slightly (0.01) compared with the fast IHS [1]. Therefore, our proposed method sacrifices a little spatial information compared with the conventional method only, not to fast IHS method. Further investigation has been done to effectively overcome this distortion.

V. BLOCK DISTORTION ON IKONOS 1-m COLOR IMAGE

The distortion of the color information had decreased compared with the other methods shown in Table III, but block distortion was seen only in the part of the edge of 1-m color image. We investigated the causes and found that this distortion corresponds to the high-frequency element of the image [36]. Here, we proposed a sharpening process using a wavelet transform [37]–[41] only to minimize or remove this block distortion in the 1-m fused MS images. This would be applied on the 1-m fused images generated by proposed fusion process described in previous paragraphs. Two images, before and after performing this process, would be compared. The block distortion at the edge in the fused images might disappear by this process.

A. Block Distortion

Some block distortions are shown on the edge enclosed with red dotted line in the part of 4×4 pixels which does not exist

(a) Fused 1m MS image (Band: R, G, B) generated by proposed technique
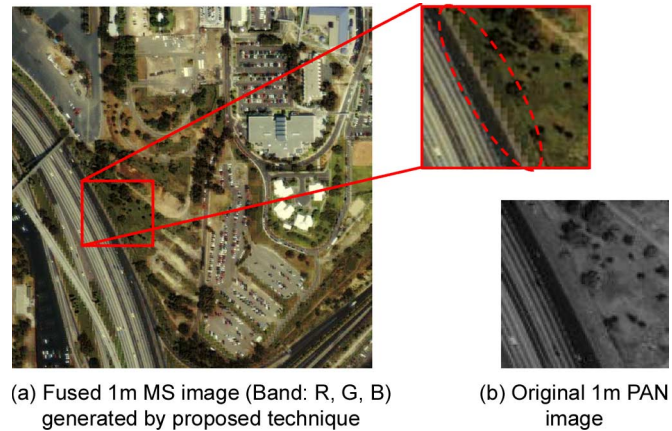
(b) Original 1m PAN image

Fig. 8. Block distortion on the IKONOS 1-m color image of (a) is enclosed with red dotted line in the part of 4×4 pixels on the upper right side. This distortion does not exist in the PAN image as shown in (b).

in the PAN image, as shown in Fig. 8. This distortion appeared because space information of PAN is not reflected perfectly in the fused image. Moreover, this distortion corresponds to the high-frequency element of the image. It is thought that the distortion might disappear by replacing the high-frequency element of the fused image with the high-frequency element of the PAN image. The wavelet-transform technique is used for replacing this high-frequency element.

B. Wavelet Transform

The wavelet transform is classified into a continuous wavelet transform and the break-up wavelet transform. A continuous wavelet transform is used for frequency analysis on a continuous signal, and the break-up wavelet transform is used for the frequency analysis on the break-up signal. The break-up wavelet transform is used in this paper. This wavelet transform can be divided into two processes: decomposition and recomposition.

The decomposition process divided the signal into signal of high- and low-frequency areas. One-dimensional signal $a[0]-a[N-1]$ is divided into low-frequency number

(a) Fused image Band: R
(after processed)

(b) Fused image Band: G
(after processed)

(c) Fused image Band: B
(after processed)

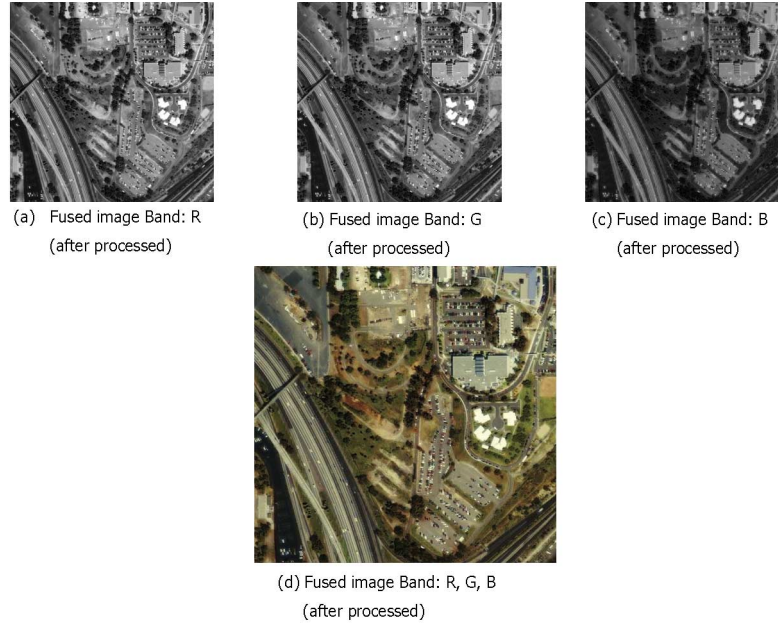(d) Fused image Band: R, G, B
(after processed)

Fig. 9.   Fused IKONOS image after sharpening processing with the wavelet transform.

element $a'[0]-a'[N/2-1]$ and high-frequency element $a'[N/2]-a'[N-1]$. This division processing can be shown by

$$a'[i] = \frac{1}{2}\left(a[2i-1] + a[2i]\right) \qquad \left(0 \leq i \leq \frac{N}{2}-1\right) \tag{23}$$

$$a'[i] = \frac{1}{2}\left(a[2i-N-1]-a[2i-N]\right) \qquad \left(\frac{N}{2} \leq i \leq N-1\right). \tag{24}$$

Here, $a[-1] = a[N-1]$.

Recomposition process is when the signal of high-frequency area and low-frequency number area is composed again, and former signal is restored. Low-frequency number element $a'[0]-a'[N/2-1]$ and high-frequency element $a'[N/2]-a'[N-1]$ are synthesized, and 1-D signal $a[0]-a[N-1]$ is composed again. This processing of the recomposition can be expressed by

$$a[2i-1] = \frac{1}{2}\left(a'[i]+a'\left[i+\frac{N}{2}\right]\right) \qquad \left(0 \leq i \leq \frac{N}{2}-1\right) \tag{25}$$

$$a[2i] = \frac{1}{2}\left(a'[i]-a'\left[i+\frac{N}{2}\right]\right) \qquad \left(0 \leq i \leq \frac{N}{2}-1\right). \tag{26}$$

VI. Proposed Sharpening Process With Wavelet Transform

Our proposed sharpening process with wavelet transform is done by using the decomposition and recomposition processes of the wavelet transform. The proposed process consists of three steps: histogram matching, decomposition, and recomposition process.

A. Histogram Matching

First, the histogram matching is processed. This generates the images named PAN_R, PAN_G, and PAN_B, with the average value and variance of PAN image matching to the average and variance of R image, G image, and B image of the fused images.

B. Decomposition Process

Next, the decomposition process is applied to the PAN_R, PAN_G, and PAN_B images that are obtained from histogram matching and also to each band of the fused images. The high-frequency elements of R, G, and B images are replaced by the high-frequency elements of PAN_R, PAN_G, and PAN_B images, respectively.

C. Recomposition Process

After the replacement, recomposition processing has been done to each band image to compose again the fused 1-m color images, and the low-frequency number element and the high-frequency element have been synthesized. The recomposed 1-m color image is shown in Fig. 9(d).

VII. Comparison of Images Before and After Performing Sharpening Process With Wavelet Transform

A good fusion method must allow addition of a high degree of spatial detail of the PAN image to the MS image.
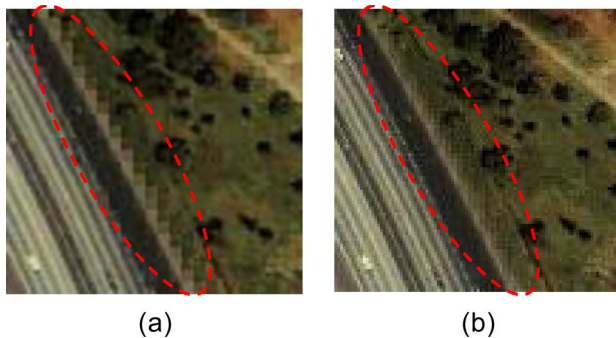
Fig. 10. Part of 4 × 4 pixels of the IKONOS 1-m color image that was generated by using the proposed fusion technique. (a) Block distortion before the sharpening process with the wavelet transform. (b) Disappearance of block distortion after the sharpening process with the wavelet transform.
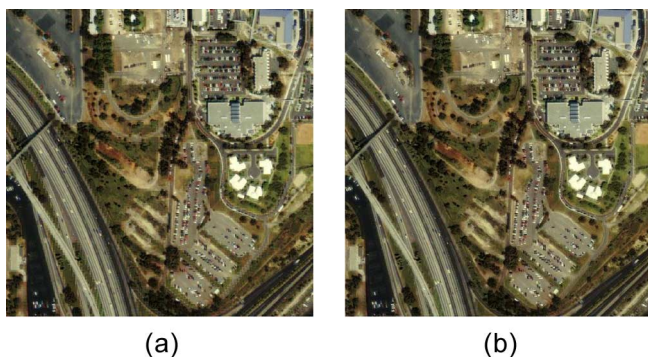

Fig. 11. IKONOS 1-m color image of San Diego, CA. The sharpening process using the wavelet transform did not significantly affect the color of the entire image before and after the sharpening process. (a) 1-m color fused image (before processed). (b) 1-m color fused image (after processed).

The addition of this spatial detail is evident for all the fused images when these are visually compared with the initial MS image [27].

The comparisons between the fused images, before and after performing this sharpening process with the wavelet transform, have been done visually and also quantitatively using the ERGAS index. It was also found that block distortion disappeared most of the cases. Fig. 10 shows an example of this comparison.

Left part of Fig. 10 shows that block distortion appeared on the part of 4 × 4 pixels of fused images before performing the sharpening process with the wavelet transform [Fig. 10(a)], and right part shows the disappearance of block distortion after performing the process [Fig. 10(b)]. This result indicates that, by the proposed sharpening process using the wavelet transform, the high-frequency element of the PAN image is reflected in the part where block distortion appeared. Block distortion also disappeared in other part of the images (Fig. 11). Moreover, color tone did not change significantly in the rest of the part of the images (Fig. 11). After performing the proposed sharpening process with the wavelet transform, the value of the ERGAS index is calculated, and it is 1.727, whereas this value was 1.384 before performing this process (Table III). Both values are lower than the value for conventional methods mentioned in Table III, which indicates better spectral and spatial quality in the fused images obtained by the proposed fusion process.

VIII. DISCUSSION

The proposed fusion process using the steepest descent method provided the 1-m fused color images with a much better spectral quality. Therefore, the spectral weighting parameters w_R, w_G, w_B, and w_{NIR} made a good tradeoff between the response of each band of MS and PAN in the fused images. However, some block effect appeared at the edge of the fused images. After the wavelet transform, this block effect has disappeared which is clearly visually understandable (Figs. 10 and 11), and spatial quality has increased with respect to the "before wavelet" as the value of r_{PAN} increased (from 0.885 to 0.898, Table III). However, the spectral quality decreased a little with respect to the "before wavelet" (from 0.920 to 0.877, Table III), which is still better than other conventional processes mentioned in Table III. These indicate that it is possible to get a better spectral quality in the fused images by sacrificing a little spatial information. On the other hand, improving the spatial quality is possible by using the proposed sharpening process with the wavelet transform on the fused images by compromising a little color distortion. After performing our proposed fusion process, the use of the sharpening process with the wavelet transform may depend on to the purpose of the application of the fused images.

IX. CONCLUSION

Our proposed fusion process using the steepest descent method has succeeded in generating the 1-m fused images where spectral distortion has been significantly reduced compared with the IHS, BT, PCA, and fast IHS fusion processes. From experimental results, it is demonstrated that the proposed fusion process performs significantly better spectral quality than the existing processes, in terms of maintaining the spectral response of the original image. However, some block distortions occurred on the part of the edge of the 1-m fused image. Our proposed sharpening process which uses the wavelet transform showed a suitable way of removing this block distortion from the fused images without a significant change in the color tone of the entire image.

REFERENCES

[1] T.-M. Tu, P. S. Huang, C.-L. Hung, and C.-P. Chang, "A fast intensity–hue–saturation fusion technique with spectral adjustment for IKONOS imagery," *IEEE Geosci. Remote Sens. Lett.*, vol. 1, no. 4, pp. 309–312, Oct. 2004.

[2] Y. Zhang and G. Hong, "An IHS and wavelet integrated approach to improve pan-sharpening visual quality of natural colour IKONOS and QuickBird images," *Inf. Fusion*, vol. 6, no. 3, pp. 225–234, Sep. 2005.

[3] R. Haydn, G. W. Dalke, and J. Henkel, "Application of the IHS color transform to the processing of multisensor data and image enhancement," in *Proc. Int. Symp. Remote Sens. Arid and Semi-Arid Lands*, Cairo, Egypt, Jan. 1982, pp. 599–616.

[4] E. Kathleen and A. D. Philip, "The use of intensity–hue–saturation transformation for producing color shaded relief images," *Photogramm. Eng. Remote Sens.*, vol. 60, no. 11, pp. 1369–1374, 1994.

[5] C. Poul and J. L. Van Genderen, "Multisensor image fusion in remote sensing: Concepts, methods and applications," *Int. J. Remote Sens.*, vol. 19, no. 5, pp. 823–854, 1998.

[6] T.-M. Tu, S.-C. , H.-C. Shyu, and P. S. Huang, "A new look at IHS-like image fusion methods," *Inf. Fusion*, vol. 2, no. 3, pp. 177–186, Sep. 2001.

[7] Y. Zhang, "A new automatic approach for effectively fusing Landsat 7 as well as IKONOS images," in *Proc. IEEE/IGARSS*, Toronto, ON, Canada, Jun. 2002, pp. 2429–2431.

[8] Y. Zhang, "Problems in the fusion of commercial high-resolution satellite images as well as LANDSAT 7 images and initial solutions," in *Proc. GeoSpatial Theory, Process. and Appl.*, 2002, vol. 34, pt. 4, pp. 9–12.

[9] W. J. Carper, T. M. Lillesand, and R. W. Kiefer, "The use of intensity–hue–saturation transformations for merging SPOT panchromatic and multispectral image data," *Photogramm. Eng. Remote Sens.*, vol. 56, no. 4, pp. 459–467, 1990.

[10] P. S. Chavez and A. Y. Kwarteng, "Extracting spectral contrast in Landsat thematic mapper image data using selective principal component analysis," *Photogramm. Eng. Remote Sens.*, vol. 55, no. 3, pp. 339–348, 1989.

[11] T. Ranchin and L. Wald, "Fusion of high spatial and spectral resolution images: The ARSIS concept and its implementation," *Photogramm. Eng. Remote Sens.*, vol. 66, no. 1, pp. 49–61, Jan. 2000.

[12] J. Nuñez, X. Otazu, O. Fors, A. Prades, V. Pala, and R. Arbiol, "Multiresolution-based imaged fusion with additive wavelet decomposition," *IEEE Trans. Geosci. Remote Sens.*, vol. 37, no. 3, pp. 1204–1211, May 1999.

[13] N. Jorge, O. Xavier, F. Octavi, and P. Albert, "Simultaneous image fusion reconstruction using wavelets application to SPOT+LANDSAT images," *Vistas Astron.*, vol. 41, no. 3, pp. 351–357, 1997.

[14] J. L. Van Genderen and C. Pohl, "Image fusion: Issues, techniques and applications. Intelligent image fusion," in *Proc. EARSeL Workshop*, J. L. Van Genderen and V. Cappellini, Eds., Strasbourg, France, Sep. 1994, pp. 18–26.

[15] G. Piella, "A general framework for multiresolution image fusion: From pixels to regions," CWI, Amsterdam, The Netherlands, Res. Rep. PNA-R0211, 2002.

[16] Z. C. Qiu, "The study on the remote sensing data fusion," *Acta Geod. Cartogr. Sin.*, vol. 19, no. 4, pp. 290–296, 1990.

[17] P. S. Chavez, Jr., S. C. Sides, and J. A. Anderson, "Comparison of three different methods to merge multiresolution and multispectral data: Landsat TM and SPOT panchromatic," *Photogramm. Eng. Remote Sens.*, vol. 57, no. 3, pp. 295–303, 1991.

[18] A. Pellemans, R. Jordans, and R. Allewijn, "Merging multispectral and panchromatic SPOT images with respect to the radiometric properties of the sensor," *Photogramm. Eng. Remote Sens.*, vol. 59, no. 1, pp. 81–87, 1993.

[19] Z. Wang, D. Ziou, C. Armenakis, D. Li, and Q. Li, "Comparative analysis of image fusion methods," *IEEE Trans. Geosci. Remote Sens.*, vol. 43, no. 6, pp. 1391–1402, Jun. 2005.

[20] Y. Zhang, "A new merging method and its spectral and spatial effects," *Int. J. Remote Sens.*, vol. 20, no. 10, pp. 2003–2014, Jul. 1999.

[21] J. Zhou, D. L. Divco, and J. A. Silander, "A wavelet transform method to merge Landsat TM and SPOT panchromatic data," *Int. J. Remote Sens.*, vol. 19, no. 4, pp. 743–757, Mar. 1998.

[22] T. A. Wilson, S. K. Rogers, and M. Kabrisky, "Perceptual based image fusion for hyperspectral data," *IEEE Trans. Geosci. Remote Sens.*, vol. 35, no. 4, pp. 1007–1017, Jul. 1997.

[23] B. Aiazzi, L. Alparone, S. Baronti, and A. Garzelli, "Context-driven fusion of high spatial and spectral resolution images based on oversampled multiresolution analysis," *IEEE Trans. Geosci. Remote Sens.*, vol. 40, no. 10, pp. 2300–2312, Oct. 2002.

[24] Y. Chibani and A. Houacine, "The joint use of IHS transform and redundant wavelet decomposition for fusing multispectral and panchromatic images," *Int. J. Remote Sens.*, vol. 23, no. 18, pp. 3821–3833, Sep. 2002.

[25] M. Lillo-Saavedra and C. Gonzalo, "Spectral or spatial quality for fused satellite imagery? A trade-off solution using the wavelet á trous algorithm," *Int. J. Remote Sens.*, vol. 27, no. 7, pp. 1453–1464, Apr. 2006.

[26] X. Otazu, M. González-Audícana, O. Fors, and J. Núñez, "Introduction of sensor spectral response into image fusion methods. Application of wavelet-based methods," *IEEE Trans. Geosci. Remote Sens.*, vol. 43, no. 10, pp. 2376–2385, Oct. 2005.

[27] M. González-Audícana, X. Otazu, O. Fors, and J. Alvarez-Mozos, "A low computational-cost method to fuse IKONOS images using the spectral response function of its sensors," *IEEE Trans. Geosci. Remote Sens.*, vol. 44, no. 6, pp. 1683–1691, Jun. 2006.

[28] P. S. Pradhan and R. L. King, "Estimation of the number of decomposition levels for a wavelet-based multiresolution multisensor image fusion," *IEEE Trans. Geosci. Remote Sens.*, vol. 44, no. 12, pp. 3674–3686, Dec. 2006.

[29] L. Alparone, S. Baronti, A. Garzalli, and F. Nencini, "A global quality measurement of Pan-Sharpened multispectral imagery," *IEEE Trans. Geosci. Remote Sens.*, vol. 1, no. 4, pp. 313–317, Apr. 2004.

[30] M. González-Audícana, J. L. Saleta, R. G. Catalán, and R. García, "Fusion of multispectral and panchromatic images using improved IHS and PCA mergers based on wavelet decomposition," *IEEE Trans. Geosci. Remote Sens.*, vol. 42, no. 6, pp. 1291–1299, Jun. 2004.

[31] T. Hjorteland, "The action variational principle in cosmology," M.S. Thesis, Inst. Theoretical Astrophysics, Univ. Oslo, Oslo, Norway, Jun. 1999.

[32] Z. Teague, "IKONOS pan-sharpened products evaluation," in *Proc. High Spatial Resolution Commercial Imagery Workshop*, Mar. 20, 2001. accessed on Aug. 3, 2005, slides 1–30. [Online]. Available: http://ldcm.gsfc.nasa.gov/library/HSRCIW01/PanSharp_ProductsEval_Teague.pdf

[33] M. Choi, "A new intensity–hue–saturation fusion approach to image fusion with a tradeoff parameter," *IEEE Trans. Geosci. Remote Sens.*, vol. 44, no. 6, pp. 1672–1682, Jun. 2006.

[34] J.-I. Kudoh, K. A. Kalpoma, and Y. Kurita, "A process to minimize the spectral distortion in 1 m IKONOS color image by using four parameters," in *Proc. IEEE Int. Geosci. and Remote Sens. Symp.*, 2006, pp. 3240–3243. (on print).

[35] J.-I. Kudoh, K. A. Kalpoma, and Y. Kurita, "An IKONOS image fusion process using steepest descent method," in *Proc. IEEE Int. Geosci. Remote Sens. Symp.*, 2006, pp. 3248–3250. (on print).

[36] J.-I. Kudoh, K. A. Kalpoma, and Y. Kurita, "An IKONOS 1 m color image fusion processing with wavelet transform," in *Proc. IEEE Int. Geosci. Remote Sens. Symp.*, 2006, pp. 3244–3247. (on print).

[37] C. K. Chui, *An Introduction to Wavelets.* New York: Academic, 1992.

[38] O. Rioul and M. Vetterli, "Wavelets and signal processing," *IEEE Signal Process. Mag.*, vol. 8, no. 4, pp. 14–38, Oct. 1991.

[39] S. G. Mallat, "A theory for multiresolution signal decomposition: The wavelet representation," *IEEE Trans. Pattern Anal. Mach. Intell.*, vol. 11, no. 7, pp. 674–693, Jul. 1989.

[40] J. P. Djamdji, A. Bijaoui, and R. Manieri, "Geometrical registration of images: The multiresolution approach," *Photogramm. Eng. Remote Sens.*, vol. 59, no. 5, pp. 645–653, 1993.

[41] T. Ranchine and L. Wald, "The wavelet transform for the analysis of remotely sensed images," *Int. J. Remote Sens.*, vol. 14, no. 3, pp. 615–619, 1993.

Kazi A. Kalpoma was born in Dhaka, Bangladesh, in 1972. She received the B.Sc. degree in applied physics and electronics and the M.Sc. degree in computer science from Dhaka University, Dhaka, in 1994 and 1996, respectively, and the Master's and Ph.D. degrees in information sciences from the Graduate School of Information Sciences, Tohoku University, Sendai, Japan, in 2000 and 2007, respectively.

Since 2002, she has been an Assistant Professor at the Department of Computer Science, American International University-Bangladesh, Dhaka. Her research interests include signal processing, image processing, and disaster monitoring using satellite image.

Jun-ichi Kudoh (A'99) received the B.S. and M.E. degrees from Mining College, Akita University, Akitafs, Japan, and the Dr. Eng. degree from Tohoku University, Sendai, Japan, in 1987, all in metallurgy.

From 1991 to 2000, he was with the Computer Center, Tohoku University, where he served as Research Associate and Associate Professor. In 2001, he moved to the Center for Northeast Asian Studies, Tohoku University, where he is currently a Professor with the Graduate School of Information Sciences. His major research field is environmental informatics, remote sensing image recognition, and database and computer network system.